Title: **Erasable Hippocampal Neural Signatures Predict Memory Discrimination**

Authors: Kinsky, Nathaniel R.,[1,3,5,6] Orlin, Daniel J.,[3,4,5] Ruesch, Evan A.[3], Diba, Kamran[1,2], Ramirez, Steve[3,6]

1 – Department of Anesthesiology, University of Michigan Medical School, Ann Arbor, MI 48109

2 – Neuroscience Graduate Program, University of Michigan, Ann Arbor, MI 48109

3 – Center for Systems Neuroscience, Boston University, Boston, MA 02451

4 – Neuroscience Graduate Program, Oregon Health & Science University, Portland, OR 97239

5 – These authors contributed equally to this work

6 – Corresponding authors. Correspondence should be addressed to N.R.K (nkinsky@umich.edu) or S.R. (dvsteve@bu.edu)

Abstract: We leveraged the spatial-temporal resolution of in vivo calcium imaging in freely moving mice to interrogate how blocking memory consolidation impacted learning-related hippocampal dynamics following contextual fear conditioning. We found that memory specificity correlated with the amount of cell turnover between a shock and neutral arena and that learning caused context-specific remapping. We induced amnesia by blocking protein synthesis following learning, which promoted an acute suppression of neural activity, and arrested learning-related place field remapping. Finally, freeze-predicting neural ensembles emerged following learning, and their coordinated activity required protein synthesis. We conclude that context-specific place field remapping and the development of coordinated ensemble activity underlie contextual fear memory consolidation.

Main Text:

The process of memory consolidation requires protein synthesis following learning to produce stable long-term memories (Barondes & Cohen, 1968; Davis & Squire, 1984; Squire & Barondes, 1974). At the synaptic level, protein synthesis is necessary for the formation of late-phase but not early-phase LTP in HPC neurons (Frey & Morris, 1997; Huang et al., 1994; Nguyen et al., 1994). Likewise, blocking protein synthesis following learning impairs long-term memory, but not short-term memory, for a hippocampus(HPC)-dependent contextual fear conditioning (CFC) task (Ryan et al., 2015; Schafe et al., 1999). These studies suggest that memory consolidation requires protein-synthesis to reinforce learning-related connections which are potentiated during CFC learning. Despite this evidence linking synaptic potentiation *in vitro* to consolidation, little is known about how protein synthesis influences the functional coding properties of neurons *in vivo* before, during, and after learning to support memory consolidation. To causally test the hypothesis that learning-related place-cell remapping (Muller & Kubie, 1987) is necessary for consolidation of a CFC memory (Moita et al., 2004; Wang et al., 2012) we combined in vivo calcium imaging in mice with systemic administration of the protein synthesis inhibitor, anisomycin, to track the evolution, remapping, and stabilization of HPC place fields during and after CFC. We further explored how between-animal variability in HPC dynamics influenced memory specificity and how blocking protein-synthesis impacted the development of HPC ensemble activity during freezing behavior.

Weeks prior to training, all mice received viral infusions of the genetically encoded calcium indicator GCaMP6f (Chen et al., 2013) in region CA1 of the dorsal hippocampus. Subsequently,

following two days of pre-exposure ("Before" learning, days -2 and -1) to an operant chamber (shock arena) and an open field (neutral arena), mice received a mild foot-shock on day 0 (training), after which they were moved to their home cage and immediately given systemic injections of either anisomycin (ANI group) or vehicle (CTRL group). We then performed a test of short-term memory 4 hours later and three tests of long-term memory 1, 2, and 7 days following training (Figure 1A), each time by measuring freezing behavior. We titrated the shock level during training such that the mice froze significantly more in the shock arena relative to the neutral arena following learning while still exploring the majority of both arenas. We observed a range of freezing levels during the day 1 and 2 memory tests (Figure S1A) and sub-divided CTRL mice into two groups: Learners, who froze significantly more in the shock arena, and Non-Learners, who either showed generalized freezing or froze at low levels in both arenas (Figures 1B, 1G, Figure S1B). Learners exhibited reduced freezing on day 7, indicative of extinction (Figure 1B). All subsequent analyses related to long-term memory therefore utilized the day 1 and 2 recall sessions ("After" consolidation). In contrast, mice in the ANI group exhibited no difference in freezing between arenas at any time point, indicating that blocking protein synthesis impaired context-specific fear memory (Figure 1C). Both the CTRL and ANI groups exhibited significant freezing in the shock arena during the 4 hour test (Figure 1D, Figure S1A), though we note that the behavior in the ANI group at this time point could arise from either contextual fear or non-specific aversive effects of anisomycin treatment (Figure S2) since these mice froze at high levels in both arenas.

We visualized the activity of pyramidal neurons in region CA1 of the dorsal hippocampus (Figure 1C) using a miniaturized epifluorescence microscope (Ghosh et al., 2011; Ziv et al., 2013). We identified a large number of neurons in each 10 minute session (n = 128 to 1216), extracted their corresponding calcium traces, and tracked them between sessions throughout the CFC task, which allowed us to determine the long-term evolution of the HPC neural code (Figure 1C,F). We next assessed behavioral expression of a CFC memory by calculating a behavioral discrimination index (DI_{beh}) to quantify how much each animal froze in the shock vs. neutral arenas. Negative DI values indicated higher freezing in the shock arena. Learners exhibited negative DI_{beh} levels on days 1 and 2 that were significantly different from both Non-Learners (by definition) and from the ANI group as well (Figure 1G). We noticed that many neurons exhibited strong changes in mean event rate between arenas (Figure 1F) and calculated a neural discrimination index (DI_{neural}) to quantify the distinctiveness of neural activity between arenas (0 = similar, 1 = distinct). Same-day neural discrimination between arenas correlated strongly with across-day neural discrimination in the same arena (Figure 1E, Figure S1C). This indicates that mice exhibit natural variability in neural discrimination which is invariant between different arenas and across time. Interestingly, we noticed that DI_{neural} was significantly higher for Learners vs. Non-Learners in the sessions *prior to* the shock (Figure 1H), indicating that inherent differences in neural discrimination influence how well mice learn the CFC task.

Previous work has demonstrated that higher overlap between HPC neurons active in two distinct arenas correlates with increased generalization or linking of a contextual fear memory across arenas (Cai et al., 2016). Accordingly, we hypothesized that the distinctiveness of the HPC neural code between arenas would predict how much mice froze in the neutral arena. We therefore utilized a regression analysis to determine if neural discrimination during memory recall *after* shock likewise correlated with memory discrimination. We utilized two metrics

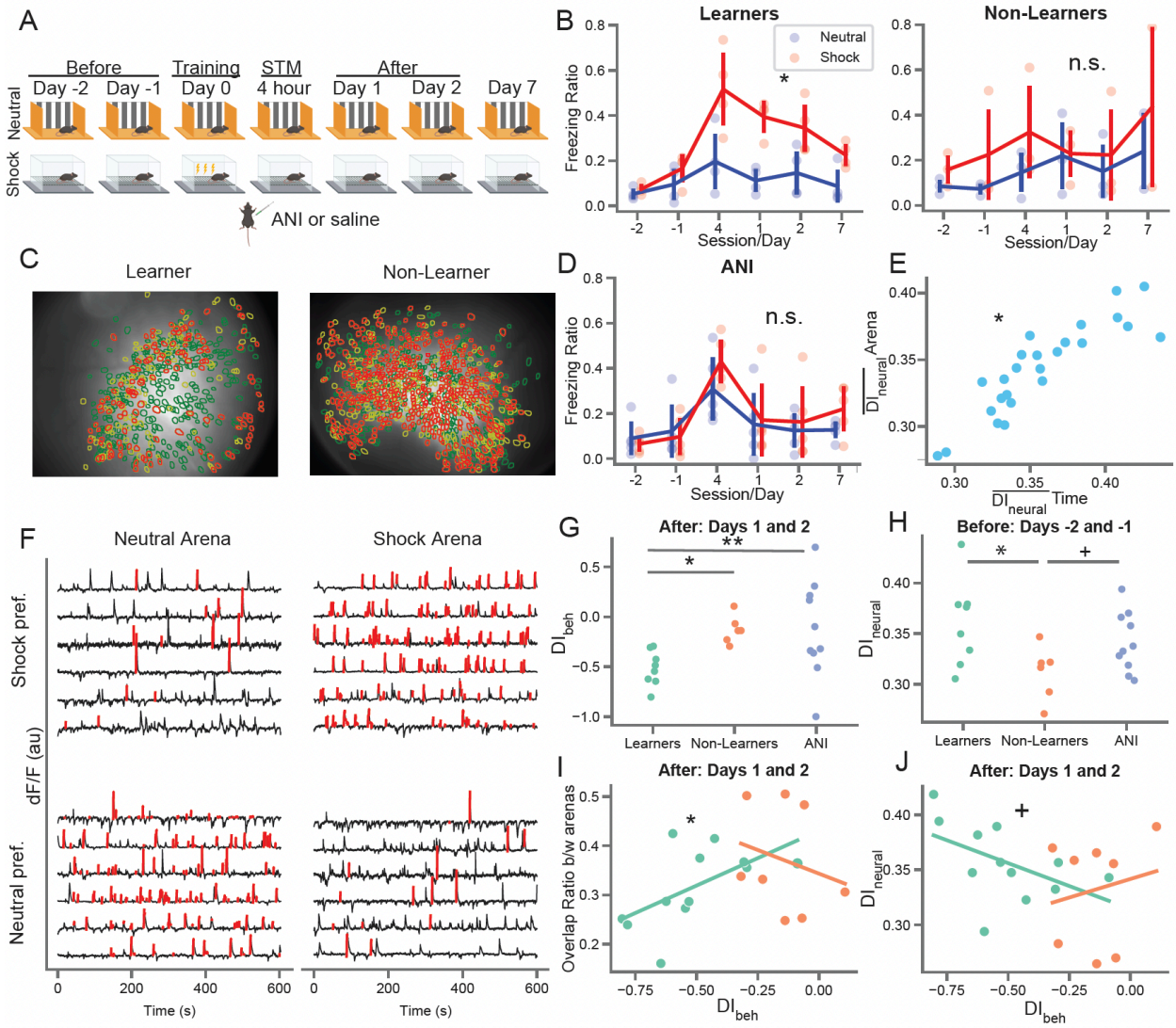

Figure 1: Neural discrimination between arenas predicts specificity of fear learning. A) Schematic of the behavioral paradigm. Mice freely explored two distinct arenas (neutral and shock) for 10 minutes each day. Mice underwent mild contextual fear conditioning on day 0 in the shock arena followed by immediate I.P. administration of anisomycin or vehicle in their home cage. Memory recall tests were conducted 4 hours and 1, 2, and 7 days post-shock. The time of each session is referenced to the shock session. **B)** (left) Learner (CTRL) mice freezing on all days. Red = shock arena, blue = neutral arena. *p=1.3e-0.5 shock **-** neutral freezing from days -2/-1 to days Ĺ one-sided t-test (n=4 mice). (right) Same but for Non-Learner (CTRL) mice (n=3 mice). **C)** (left) Neural overlap plots between neutral and shock arenas for an example Learner mouse on day -1, before shock. Green = cells active in the shock arena only, yellow = cells active in the neutral arena only, orange = cells active in both arenas. (right) Same for example Non-Learner on day -2 showing higher overlap of active cells between arenas. **D)** Same as B but for ANI group **E)** Mean neural discrimination between arenas (same day, days -2 to -1 and 1 to 2) vs. within arenas (same arena, days -2 and -1, days 1 and 2). *p=2.35e-8 (ρ=-0.56) Spearman correlation. **F)** Example calcium activity from the Learner mouse shown in C (left) for cells active in both arenas. Black = calcium trace, red = putative spiking activity during transient rises. Top row shows shock arena preferring cells, bottom row shows neutral arena preferring cells. **G)** Behavioral discrimination between arenas after shock (Days 1-2) shows formation of a specific fear memory for Learners only, by definition (positive = more freezing in neutral arena, negative = more freezing in shock arena, 0 = equal freezing in both arenas). *p=0.022, **p=0.00038 1-sided t-test **H)** Neural discrimination between arenas BEFORE shock indicates Learners formed more distinct representations of each arena prior to learning. Same conventions as F. *p=0.030, +p=0.059 two-sided t-test. **I)** Neural overlap between arenas correlates with specificity of fear memory on days 1-2 for Learners but not Non-Learners. *p=0.033 (ρ=0.61). **J)** Same as I) but plotting neural overlap vs. behavioral discrimination between arenas. +p=0.059 (ρ=-0.56) for Learners.

to quantify the distinctiveness of the HPC neural code between arenas: 1) the overlap ratio of neurons active in both arenas divided by the total number of cells active in either arena, which accounts for cells that may be silent in one of the arenas, and 2) the aforementioned DI_{neural} metric, which is based on the cells that are active in both arenas. We found that overlap ratio

was significantly correlated with DI_{beh} for Learners, but not for Non-Learners, on days 1-2 (Figure 1I); likewise, the correlation between DI_{beh} and DI_{neural} approached significance for Learners but not for Non-Learners on days 1-2 (Cai et al., 2016; Figure 1J). Together, our results indicate that mice with segregated experiences in the HPC neural code were more capable of forming discrete long-term memories and that the distinctiveness of the HPC calcium activity predicts the specificity of memory for CFC.

Next, we probed how arresting protein synthesis impacted HPC dynamics. We hypothesized that, by preventing plasticity, ANI administration would slow or stop the normal rate of cell turnover observed across days (Figure 2A). Surprisingly, we found that ANI administration rapidly accelerated the turnover in which cells are active at any given time. This “cell turnover” was indicated by lower overlap of active cells from experiment start to the 4 hour session in the ANI group compared to the CTRL group (Figure 2A-C). This effect appeared to be driven by a sharp decrease in the number of active neurons in the ANI group at the 4 hour session following administration of ANI, despite these mice displaying comparable levels of freezing to CTRL mice at this time point (Figure 2D). Interestingly, this accelerated turnover in cells was only temporary and was followed by a decrease in the cell turnover rate from the 4 hour to day 1 session for ANI compared to CTRL mice (Figure 2B-C). Importantly, we observed no difference in the mean height of calcium transients for neurons active before, during, or after ANI administration, indicating that the observed decrease in the number of active neurons was not due to differences in Ca2+ levels or depletion of the GCaMP protein (Figure S7D-E). To confirm that this decrease in activity was not due to suppression of network activities, such as those reported for intracranial infusions of protein synthesis inhibitors in anesthetized or immobile rodents (Barondes & Cohen, 1966; Sharma et al., 2012), we performed extracellular recordings in a freely-moving rat implanted with a linear probe in the CA1 region of the hippocampus following administration of anisomycin. We observed preserved theta activity, theta modulation of spiking, as well as robust sharp wave ripple activity for up to 5 hours following anisomycin administration (Figure S7A-C). These observations therefore indicate that blocking protein synthesis following learning does not abolish all neuronal activity but instead reduces of the number of active neurons, which may be those specifically involved in learning.

We next hypothesized that arresting protein synthesis, which disrupts the permanence of newly formed place fields (Agnihotri et al., 2004), would likewise impair the long-term stability of CFC-related remapping (Moita et al., 2004; Wang et al., 2012). We therefore assessed place field remapping within and across epochs by correlating event rate maps for all neurons active between two sessions (Figure 2E-F) following administration of anisomycin vs. saline. We noticed that place fields recorded in the Learners group exhibited very low across-session correlations in the neutral arena throughout the experiment (Figure S3), which could indicate remapping. However, in a separate study, we observed what appeared to be remapping but what was actually a coherent rotation of all place fields between two recording sessions (Kinsky et al., 2018). This manifests when all place fields rotate to the same degree around a singular point, indicative of confusion in an animal’s axis of orientation, such as between west and north (Keinath et al., 2017). Importantly, such angular disorientation does not impair the ability of mice to identify specific places (Julian et al., 2015), and between-cell firing relationships are maintained during coherent rotations whereas they are scrambled following remapping. Coherent rotations match the geometry of the environment, e.g. producing rotations in 60 degree increments in a triangle versus 90 degrees in a square. Therefore, since both shock and neutral arenas were square, we rotated maps from each session in 90 degree increments and

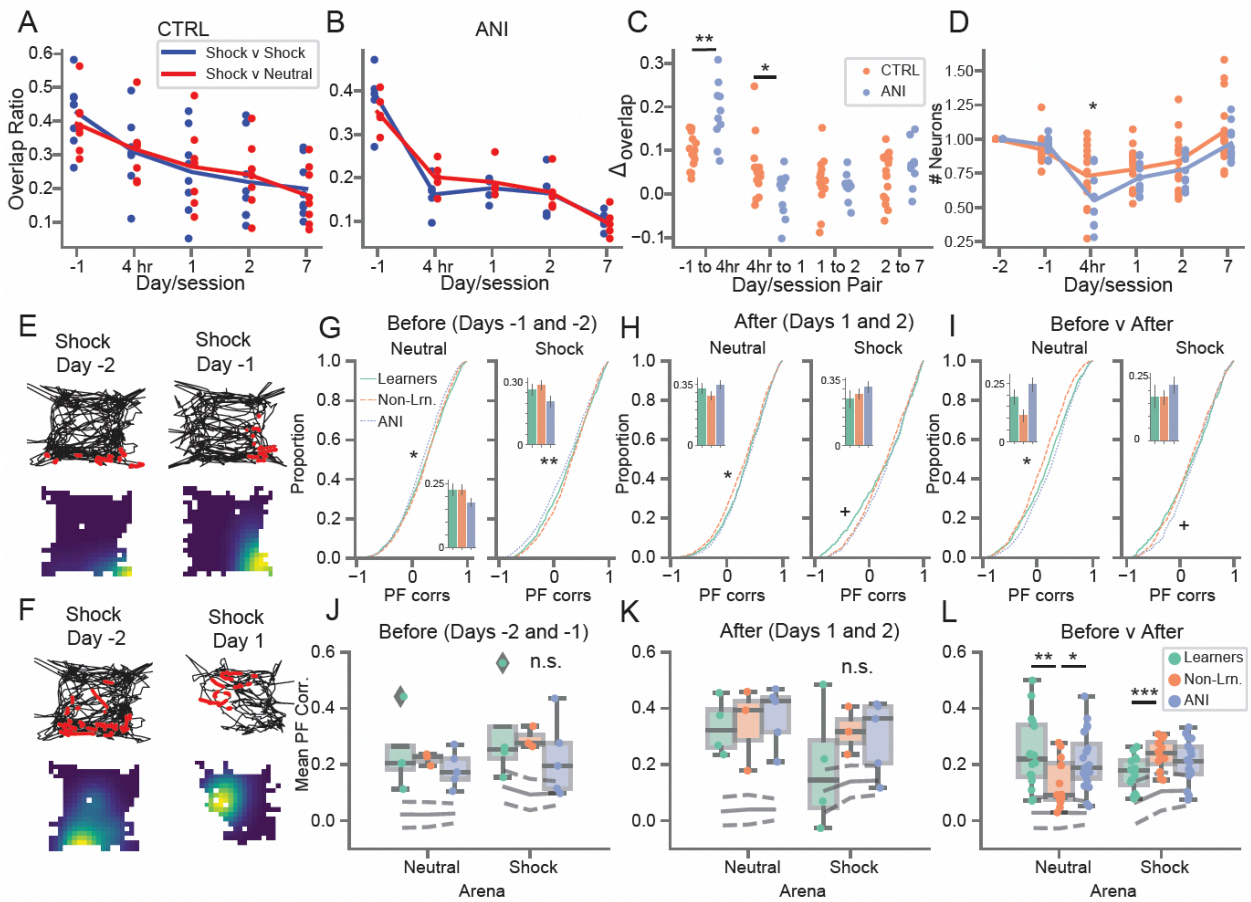

Figure 2: Anisomycin accelerates cell turnover and stifles learning-related place field remapping A) Cell overlap ratio with Day -2 session, CTRL group. Blue = within shock arena, red = shock v. neutral arena. **B)** Same as A) but for ANI group. **C)** Change in overlap ratios from a and b. *p=0.028, **p=0.00024 two-sided t-test. **D)** Number of active neurons observed each day, normalized to day -1. *p=0.039 two-sided t-test. **E)** Stable place field. (top) Example mouse trajectory (black) with calcium activity (red) overlaid for the same cell from day -2 to -1 in shock arena, (bottom) occupancy normalized rate maps for the same cells. **F)** Remapping place field. Same as E) but for a different cell that remaps from day -2 to day 1 in the shock arena. **G)** Place field correlations for all mice before shock (Days -2 and -1). *p<0.0032 Learners vs ANI and Non-Learners vs ANI, **p=1.9e-6 Non-Learners vs ANI, k-s test after Bonferroni correction. **H)** Same as G) but for days after shock. *p=0.045 Learners vs Non-Learners and p=0.0059 Non-Learners vs ANI, +p=0.1 Learners vs ANI. **I)** Same as G) but to assess learning-related remapping from before to after shock. *p=0.00021 Learners vs Non-Learners and p=3.4e-11 Non-Learners vs ANI, +p=0.12 Learners vs ANI. **J)** Place field correlations before shock broken down by mouse. **K)** Same as J) but for sessions after shock. **L)** Same as J) but from before to after shock. p=0.002 mixed ANOVA, group x arena interaction. *p=0.025 Non-Learners vs ANI, **p=0.013 Learners vs Non-Learners, ***p=0.034 Learners vs ANI, post-hoc pairwise t-test after Bonferroni correction.

used only the orientation that produced the highest correlation between sessions. We found generally higher correlations compared to using non-rotated maps (Figure 2G-H, J-K vs. Figure S3F-G), confirming that coherent rotations occurred in many recording sessions. In particular, place field correlations were high both before learning and after consolidation (Figure 2J-K), though Learner correlations trended toward lower stability after shock (Figure 2H,K). We then compared place fields from before to after learning to assess learning-related remapping. In agreement with previous studies (Moita et al., 2004; Wang et al., 2012), Learner place fields remapped, as indicated by lower correlations in the shock arena compared to the other groups (Figure 2I,L). Interestingly, compared to the other groups, Non-Learners exhibited lower place map correlations in the neutral arena, indicating paradoxically stable place fields in the shock arena but remapping in the neutral arena (Figure 2I,L). If learning causes remapping, this double dissociation indicates that Non-Learner memory deficits might result from improperly associating the neutral arena with shock. In contrast, the place maps of mice in the ANI group

displayed high correlations in all arenas, including after learning. This deficit in remapping following anisomycin therefore indicates that protein synthesis is required to stabilize the set of place fields which emerge following learning to support memory consolidation. Overall, these observations indicate that remapping is necessary for the creation of context-specific memories and that a lack of remapping or improperly remapping may underlie the memory deficits observed in Non-Learners and in the ANI group.

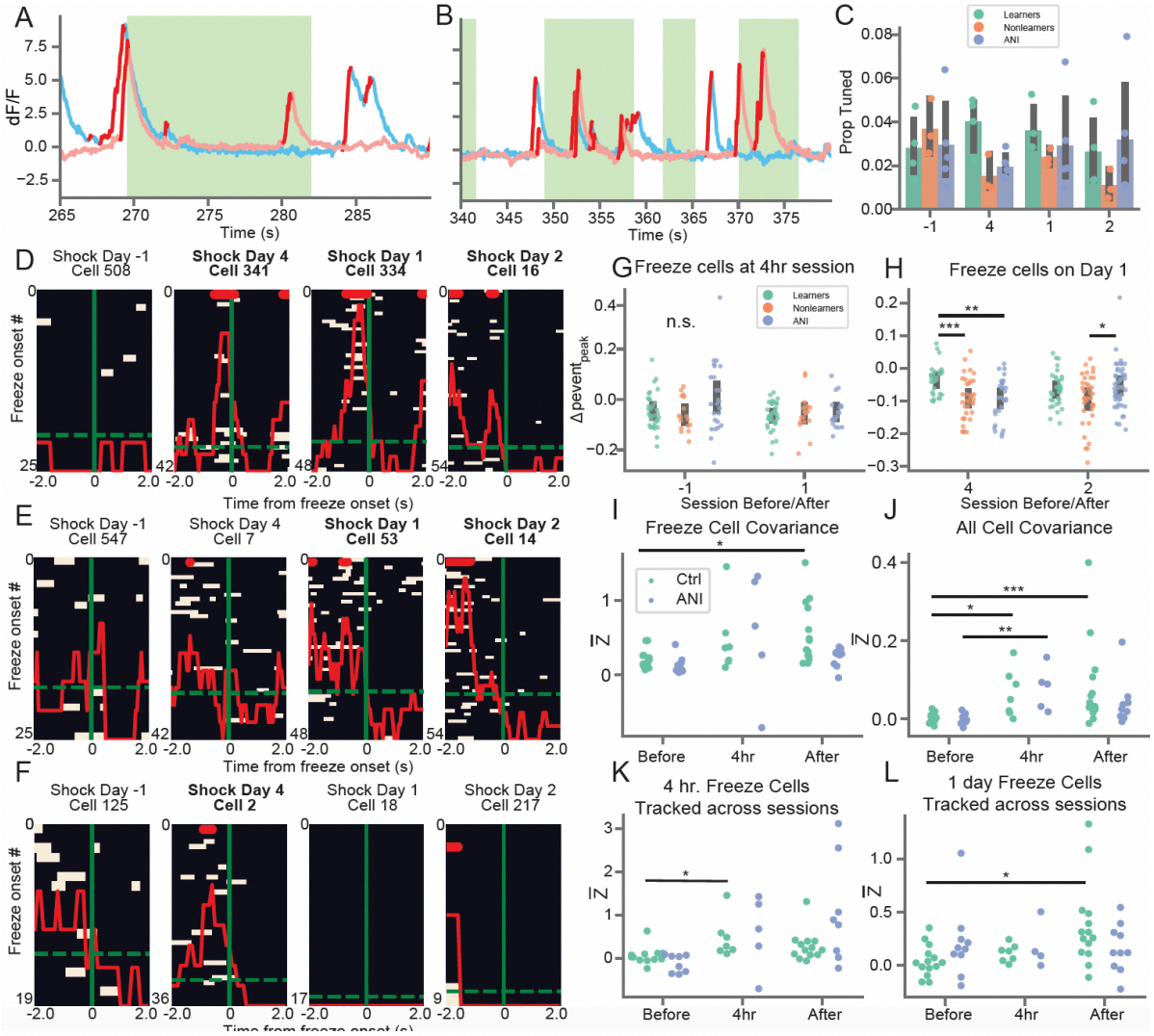

Figure 3: ANI administration suppresses the development of coordinated freeze-related neural activity. A) and B) Example traces from two freeze-cells which exhibit coordinated activity prior to freezing event during the day 1 memory recall session in the shock arena. Red = putative spiking activity, pink = cell shown in C, blue = cell shown in E. **C)** Proportion of freeze-tuned cells detected each day across all groups. Green = freezing epochs. **D) and E)** Example Learner freeze-tuned cells identified during the 4 hour (D) or day 1 (E) memory test tracked across sessions. Peri-event calcium activity rasters are centered on freeze onset time (solid green). Dashed green = baseline calcium event probability, red solid = peri-freeze calcium event probability, bins with p<0.01 (circular permutation test) noted with red bars at top. D/E corresponds to pink/blue cells shown in A-B. Bold = session with significant freeze-tuning. **F)** Same as D and E but for ANI mouse shock cell identified during the 4 hour session. **G)** Change in peak peri-freeze calcium event probability for all freeze-tuned cells detected during the 4 hour session. **H)** Same as G but for freeze-tuned cells detected during Day 1 recall session. p < 0.02 1-way ANOVA each day separately, *p=0.02, **p=0.001, ***p=0.0006 post-hoc Tukey test. **I)** Freeze-tuned cells exhibit increased covariance in the CTRL compared to the ANI group. Mean covariance of freeze-tuned cells from each session shown. p=0.016 two-way ANOVA (Time). *p=0.018 post-hoc pairwise t-test (two-sided) after Bonferroni correction. **J)** Small but significant increase in covariance of all cells for CTRL mice during the 1 day recall session. p=0.0015 (Time), 0.005 (Group), 0.036 (Group x Time) two-way ANOVA. *p=0.014, **p=0.008, ***p=0.004 post-hoc pairwise t-test (two-sided) after Bonferroni correction. **K)** Mean covariance of freeze-tuned cells detected during the 4 hour session tracked across sessions. P=0.005 (Group), 0.04 (Group x Time) two-way ANOVA. *p=0.014 post-hoc pairwise t-test (two-sided) after Bonferroni correction. **L)** Same as K but for freeze-tuned cells detected during the day 1 recall session. p=0.0003 (Group) two-way ANOVA. *p=0.016 post-hoc pairwise t-test (two-sided) after Bonferroni correction.

In addition to the spatial code, hippocampal neural activity also reflects non-spatial variables in a task (McKenzie et al., 2014; Muzzio et al., 2009; Wood et al., 1999). We noticed that many hippocampal neurons exhibited calcium transients around the time that mice froze (Figure 3A-B, Figure S6A-C) in line with recent studies (Lee & Han, 2022; Schuette et al., 2020). Neurons which exhibited a significant increase in calcium event probability +/- 2 sec from a freezing epoch we therefore dubbed freeze-tuned cells (Figure 3D-F). We observed similar proportions of freeze-tuned cells across all groups and recording sessions, even before CFC (Figure 3C, Figure S6D). However, we noticed that freeze-tuned cells appeared to activate more reliably around freezing epochs following CFC for Learners compared to similar immobility epochs in Non-Learners and in the ANI group (Figure 3D-E vs. Figure 3F and Figure S6B-C). Therefore, CFC learning may cause an increase in the reliable firing of previously identified immobility signaling cells, as primarily seen in CA2, but also in CA1 (Kay et al., 2016).

To quantify changes in within-cell freeze-turning reliability, we tracked the peak, peri-freeze calcium event probability of each freeze cell backwards and forwards in time from the 4 hour recall session. We hypothesized that freeze-tuning reliability would increase immediately following learning at the 4 hour session and remain stable thereafter (see Figure 3D). Surprisingly, freeze-tuning reliability did not significantly change from the day before to the day after the 4 hour session for any group (Figure 3G). However, when we tracked cells backward and forward from the subsequent day 1 recall session, we found that freeze cells exhibited much higher tuning stability spanning from the 4 hour recall to the day 2 recall sessions in Learners than did these cells in other groups (Figure 3H). This indicates that in Learners, reliable freeze-tuning begins to emerge between 4 hours and 1 day following learning and was maintained thereafter (see Figure 3E for exemplar cell). In contrast, freeze-tuning in mice from the ANI group and Non-Learners was more transient and unreliable across all time spans.

Lastly, we investigated whether the higher reliability of freeze-cells in Learners translated to increased co-activity (see Figure 3A-B) in this neuronal subpopulation. Freeze-cell covariance increased incrementally starting at the 4 hour session for all mice; covariance remained high on days 1 and 2 for the CTRL group (Learner and Non-Learners combined) but returned to baseline for mice in the ANI group (Figure 3I). A similar increase in covariance for the CTRL group was also observed across all cells (Figure 3J). These effects were driven by increased covariance for Learners but not Non-Learners (Figure S6J-K). Importantly, the ANI group also displayed increased covariance between all cells at the 4 hour session, but not at subsequent time points which have been shown to require post-learning protein synthesis for consolidation. We observed consistent results when we downsampled the number of freezing events following learning to match that on days -2 and -1 (Figure S6F-G). For freeze cells, but not all cells, the increased covariance was driven by peri-freeze neural activity (Figure S6H-I). In these analyses we compared freeze-cells identified independently on each day of the experiment. We next performed additional analyzes focused on the same set of freeze-tuned cells conditioned on their activity in specific sessions. Freeze-cells identified at the 4 hour session displayed increased covariance from the days before training for the CTRL, but not the ANI group (Figure 3K). Freeze-cells that were identified on the day 1 recall test exhibited increased covariance on days 1 and 2 for the CTRL, but not the ANI group (Figure 3L). However, these cells did not exhibit increased covariance during the previous day's 4 hour session, indicating that even though freeze-tuning begins to emerge immediately following learning, cell connections continue to reorganize further to form coordinated ensembles. These results indicate that freeze-related tuning emerges following learning and continues to take shape in the ensuing hours until it

stabilizes one day later. Importantly, the coordination of these freeze-tuned cells into neuronal ensembles requires protein synthesis.

Conclusions:

The results of our study provide evidence that HPC spatial representations support contextual memory formation and consolidation. We found that between-arena neural overlap correlated strongly with across-day neural overlap (Figure 1E), suggesting that the neural basis for contextual discrimination and representational drift may share the same mechanism (Hainmueller & Bartos, 2018; Kinsky et al., 2020; Mankin et al., 2012). This inherent neural variability in HPC neuron dynamics *prior to learning* impacts the specificity of contextual fear memory (Figure 1H). Based on these observations, we propose that the ability of the HPC to form distinct representations of two arenas despite overlapping contextual qualities allows for the formation of discrete contextual memories that could underlie why some mice learn while others do not. Conversely, the similarity of neural representations *after consolidation* could serve as a biological signature of memory generalization (Figure 1I). We saw that anisomycin acutely suppressed the number of active cells immediately following learning (Figure 2D). Given that remapping is observed in Learners during this time window, we speculate that arresting protein synthesis may temporarily block the formation of new place-fields in the subset of cells that undergo remapping following CFC, potentially by preventing the formation and strengthening of new neuronal connections. This idea is resonant with the notion that more excitable/active neurons are preferentially involved in memory trace formation (Rashid et al., 2016; Sweis et al., 2021). While such reduced activity could also potentially result from the blockage of constitutive protein translation (Scavuzzo et al., 2019), our study does not support this view as we did not observe a global shutdown of neural activity (Figure S7). In addition to this suppression, anisomycin's amnestic effects coincided with a reduction in learning-related remapping, effectively halting HPC contextual representations in their prior state (Figure 2L).

Lastly, we confirm that a subset of hippocampal cells exhibits freeze tuning following fear conditioning (Schuette et al., 2020) and that the organization of these cells into reliable, co-active neuronal ensembles increases following learning (Lee & Han, 2022) and requires protein synthesis (Figure 3H-I). Importantly, covariance increased incrementally for both ANI and CTRL groups at the 4 hour recall session, a time point at which protein synthesis is not required for the induction of (early-phase) long-term potentiation *in vitro* (Frey & Morris, 1997; Nguyen et al., 1994). However, at later time points, when protein synthesis *is* required to maintain (late-phase) long-term potentiation (Frey et al., 1993; Nguyen et al., 1994), between-cell covariance remained high for the CTRL group only (Figure 3G-J). Therefore, in addition to maintaining learning-related synaptic changes over hours to days, protein synthesis might also be instrumental for producing coordinated firing of large groups of neurons. A previous study demonstrated that synchronous optogenetic stimulation of engram neurons tagged during learning could artificially reactivate a fear memory even when normal long-term recall of the fear memory was blocked by anisomycin (Ryan et al., 2015). Our results provide a parsimonious explanation for these results by demonstrating that anisomycin halts the co-firing of freeze-tuned cells, weakening the capacity of these neurons to transmit behavior-related information to downstream regions through coincident firing (Lisman, 1997) and impairing their ability to trigger memory recall (Ryan & Frankland, 2022). Future work will disentangle the differential contributions that halting protein synthesis versus suppressing neural activity play in disrupting memory consolidation.

Overall, our results indicate that protein synthesis is necessary for forming new stable spatial representations of an aversive context following learning and for producing coordinated activity of freeze-tuned neurons.

Acknowledgments: First and foremost, we would like to thank Howard Eichenbaum who helped conceive and design this study before his unfortunate passing in 2017. We would also like to thank Sam McKenzie for his help during early experimental design. We would like to thank Michael Hasselmo and Ian Davison for their support and feedback while performing the recordings for this study. Next, we thank Sam Levy, Dave Sullivan, and Will Mau for their assistance in all phases of calcium imaging throughout. We would like to thank Zach Pennington for valuable feedback concerning anisomycin preparation and administration, and Denise Cai and Lucas Carstensen for analysis suggestions. We would like to thank Pho Hale, Rachel Wahlberg, and Utku Kaya for feedback on the manuscript. We would like to acknowledge the GENIE Program, specifically Vivek Jayaraman, PhD, Douglas S. Kim, PhD, Loren L. Looger, PhD, Karel Svoboda, PhD from the GENIE Project, Janelia Research Campus, Howard Hughes Medical Institute, for providing the GCaMP6f virus. Finally, we would like to acknowledge Inscopix, Inc. for making single-photon calcium imaging miniscopes widely available, and specifically Lara Cardy and Vardhan Dani for all their technical support throughout the experiment. This work was supported by NIH Grants R01 MH052090, R01 MH051570, R01MH117964, NIH NRSA Fellowship 1F32NS117732-01, NIH Early Independence Award DP5 OD023106-01, an NIH Transformative R01 Award, a Young Investigator Grant from the Brain and Behavior Research Foundation, a Ludwig Family Foundation grant, and the McKnight Foundation Memory and Cognitive Disorders award, and Boston University's Neurophotonics Center,

References

Agnihotri, N. T., Hawkins, R. D., Kandel, E. R., & Kentros, C. G. (2004). The long-term stability of new hippocampal place fields requires new protein synthesis. *Proceedings of the National Academy of Sciences*, *101*(10), 3656–3661. https://doi.org/10.1073/pnas.0400385101

Barondes, S. H., & Cohen, H. D. (1966). Puromycin Effect on Successive Phases of Memory Storage. *Science*, *151*(3710), 594–595. https://doi.org/10.1126/science.151.3710.594

Barondes, S. H., & Cohen, H. D. (1967). Delayed and Sustained Effect of Acetoxycycloheximide on Memory in Mice. *Proceedings of the National Academy of Sciences of the United States of America*, *58*, 157–164.

Barondes, S. H., & Cohen, H. D. (1968). Memory impairment after subcutaneous injection of acetoxycycloheximide. *Science (New York, N.Y.)*, *160*(3827), 556–557. http://www.ncbi.nlm.nih.gov/pubmed/5689416

Cai, D. J., Aharoni, D., Shuman, T., Shobe, J., Biane, J., Lou, J., Kim, I., Baumgaertel, K., Levenstain, A., Tuszynski, M., Mayford, M., & Silva, A. J. (2016). A shared neural ensemble links distinct contextual memories encoded close in time. *Nature*, *534*, 115–118. https://doi.org/10.1038/nature17955

Chen, T.-W., Wardill, T. J., Sun, Y., Pulver, S. R., Renninger, S. L., Baohan, A., Schreiter, E. R., Kerr, R. a, Orger, M. B., Jayaraman, V., Looger, L. L., Svoboda, K., & Kim, D. S. (2013).

Ultrasensitive fluorescent proteins for imaging neuronal activity. *Nature*, *499*(7458), 295–300. https://doi.org/10.1038/nature12354

Davis, H. P., & Squire, L. R. (1984). Protein synthesis and memory: A review. *Psychological Bulletin*, *96*(3), 518–559. https://doi.org/10.1037/0033-2909.96.3.518

Frey, U., Huang, Y.-Y., & Kandel, E. R. (1993). Effects of cAMP Simulate a Late Stage of LTP in Hippocampal CA1 Neurons. *Science*, *260*(5114), 1661–1664. https://doi.org/10.1126/science.8389057

Frey, U., & Morris, R. G. M. (1997). Synaptic tagging and long-term potentiation. *Nature*, *385*(6616), 533–536. https://doi.org/10.1038/385533a0

Frey, U., & Morris, R. G. M. (1998). Synaptic tagging: Implications for late maintenance of hippocampal long- term potentiation. *Trends in Neurosciences*, *21*(5), 181–188. https://doi.org/10.1016/S0166-2236(97)01189-2

Ghosh, K. K., Burns, L. D., Cocker, E. D., Nimmerjahn, A., Ziv, Y., Gamal, A. el, & Schnitzer, M. J. (2011). Miniaturized integration of a fluorescence microscope. *Nature Methods*, *8*(10), 871–878. https://doi.org/10.1038/nmeth.1694

Hainmueller, T., & Bartos, M. (2018). Parallel emergence of stable and dynamic memory engrams in the hippocampus. *Nature*, *558*(7709), 292–296. https://doi.org/10.1038/s41586-018-0191-2

Huang, Y. Y., Li, X. C., & Kandel, E. R. (1994). cAMP contributes to mossy fiber LTP by initiating both a covalently mediated early phase and macromolecular synthesis-dependent late phase. *Cell*, *79*(1), 69–79. https://doi.org/10.1016/0092-8674(94)90401-4

Julian, J. B., Keinath, A. T., Muzzio, I. A., & Epstein, R. A. (2015). Place recognition and heading retrieval are mediated by dissociable cognitive systems in mice. *Proceedings of the National Academy of Sciences*, *112*(20), 6503–6508. https://doi.org/10.1073/pnas.1424194112

Kay, K., Sosa, M., Chung, J., Karlsson, M. P., Larkin, M., Grossrubatscher, I., & Frank, L. M. (2016). A hippocampal network for spatial coding during immobility. *Nature*, *531*, 185–190. https://doi.org/10.1038/nature17144

Keinath, A. T., Julian, J. B., Epstein, R. A., & Muzzio, I. A. (2017). Environmental Geometry Aligns the Hippocampal Map during Spatial Reorientation. *Current Biology*, *27*(3). https://doi.org/http://dx.doi.org/10.1016/j.cub.2016.11.046

Kinsky, N. R., Mau, W., Sullivan, D. W., Levy, S. J., Ruesch, E. A., & Hasselmo, M. E. (2020). Trajectory-modulated hippocampal neurons persist throughout memory-guided navigation. *Nature Communications*, 1–14. https://doi.org/10.1038/s41467-020-16226-4

Kinsky, N. R., Sullivan, D. W., Mau, W., Hasselmo, M. E., & Eichenbaum, H. B. (2018). Hippocampal Place Fields Maintain a Coherent and Flexible Map across Long Timescales. *Current Biology*, *28*(22), 1–11. https://doi.org/10.1016/J.CUB.2018.09.037

Lee, H.-S., & Han, J.-H. (2022). Activity patterns of individual neurons and ensembles correlated with retrieval of a contextual memory in the dorsal CA1 of mouse hippocampus. *The*

Journal of Neuroscience, *43*(1), JN-RM-1407-22. https://doi.org/10.1523/jneurosci.1407-22.2022

Lisman, J. E. (1997). Bursts as a unit of neural information: Making unreliable synapses reliable. *Trends in Neurosciences*, *20*(1), 38–43. https://doi.org/10.1016/S0166-2236(96)10070-9

Mankin, E. A., Sparks, F. T., Slayyeh, B., Sutherland, R. J., Leutgeb, S., & Leutgeb, J. K. (2012). Neuronal code for extended time in the hippocampus. *Proceedings of the National Academy of Sciences*, *109*(47), 19462–19467. https://doi.org/10.1073/pnas.1214107109/-/DCSupplemental.www.pnas.org/cgi/doi/10.1073/pnas.1214107109

Mau, W., Sullivan, D. W., Kinsky, N. R., Hasselmo, M. E., Howard, M. W., & Eichenbaum, H. B. (2018). The Same Hippocampal CA1 Population Simultaneously Codes Temporal Information over Multiple Timescales. *Current Biology*, *28*(10), 1499-1508.e4. https://doi.org/10.1016/j.cub.2018.03.051

McKenzie, S., Frank, A. J., Kinsky, N. R., Porter, B., Rivière, P. D., & Eichenbaum, H. B. (2014). Hippocampal representation of related and opposing memories develop within distinct, hierarchically organized neural schemas. *Neuron*, *83*(1), 202–215. https://doi.org/10.1016/j.neuron.2014.05.019

Moita, M. A. P., Rosis, S., Zhou, Y., LeDoux, J. E., & Blair, H. T. (2004). Putting Fear in Its Place: Remapping of Hippocampal Place Cells during Fear Conditioning. *Journal of Neuroscience*, *24*(31), 7015–7023. https://doi.org/10.1523/JNEUROSCI.5492-03.2004

Muir, D. R., & Kampa, B. M. (2015). FocusStack and StimServer: a new open source MATLAB toolchain for visual stimulation and analysis of two-photon calcium neuronal imaging data. *Frontiers in Neuroinformatics*, *8*(January), 1–13. https://doi.org/10.3389/fninf.2014.00085

Muller, R. U., & Kubie, J. L. (1987). The effects of changes in the environment on the spatial firing of hippocampal complex-spike cells. *The Journal of Neuroscience*, *7*(7), 1951–1968. http://www.ncbi.nlm.nih.gov/pubmed/3612226

Muzzio, I. A., Levita, L., Kulkarni, J., Monaco, J. D., Kentros, C. G., Stead, M., Abbott, L. F., & Kandel, E. R. (2009). Attention enhances the retrieval and stability of visuospatial and olfactory representations in the dorsal hippocampus. *PLoS Biology*, *7*(6). https://doi.org/10.1371/journal.pbio.1000140

Nguyen, P., Abel, T., & Kandel, E. R. (1994). Requirement of a critical period of transcription for induction of a late phase of LTP. *Science*, *265*(5175), 1104–1107. https://doi.org/10.1126/science.8066450

Olypher, A. v, Lánský, P., Muller, R. U., & Fenton, A. A. (2003). Quantifying location-specific information in the discharge of rat hippocampal place cells. *Journal of Neuroscience Methods*, *127*(2), 123–135. https://doi.org/10.1016/S0165-0270(03)00123-7

Rashid, A. J., Yan, C., Mercaldo, V., Hsiang, H. L., Park, S., Cole, C. J., Cristofaro, A. de, Yu, J., Ramakrishnan, C., Lee, S. Y., Deisseroth, K., Frankland, P. W., & Josselyn, S. A. (2016). Competition between engrams influences fear memory formation and recall. *Science*, *353*(6297), 383–388. https://doi.org/10.1126/science.aaf0594

Resendez, S. L., Jennings, J. H., Ung, R. L., Namboodiri, V. M. K., Zhou, Z. C., Otis, J. M., Nomura, H., McHenry, J. A., Kosyk, O., & Stuber, G. D. (2016). Visualization of cortical, subcortical and deep brain neural circuit dynamics during naturalistic mammalian behavior with head-mounted microscopes and chronically implanted lenses. *Nature Protocols*, *11*(3), 566–597. https://doi.org/10.1038/nprot.2016.021

Ryan, T. J., & Frankland, P. W. (2022). Forgetting as a form of adaptive engram cell plasticity. *Nature Reviews Neuroscience*, *23*(3), 173–186. https://doi.org/10.1038/s41583-021-00548-3

Ryan, T. J., Roy, D. S., Pignatelli, M., Arons, A., & Tonegawa, S. (2015). Engram cells retain memory under retrograde amnesia. *Science*, *348*(6238), 1007–1013. https://doi.org/10.1126/science.aaa5542

Scavuzzo, C. J., LeBlancq, M. J., Nargang, F., Lemieux, H., Hamilton, T. J., & Dickson, C. T. (2019). The amnestic agent anisomycin disrupts intrinsic membrane properties of hippocampal neurons via a loss of cellular energetics. *Journal of Neurophysiology*, *122*(3), 1123–1135. https://doi.org/10.1152/jn.00370.2019

Schafe, G. E., Nadel, N. v., Sullivan, G. M., Harris, A., & LeDoux, J. E. (1999). Memory consolidation for contextual and auditory fear conditioning is dependent on protein synthesis, PKA, and MAP kinase. *Learning and Memory*, *6*(2), 97–110. https://doi.org/10.1101/lm.6.2.97

Schuette, P. J., Reis, F. M. C. V., Maechler, P., Chakerian, M., Torossian, A., Blair, G., Wang, W., Blair, H. T., Fanselow, M. S., Kao, J. C., & Adhikari, A. (2020). Long-term characterization of hippocampal remapping during contextual fear acquisition and extinction. *The Journal of Neuroscience*, *September*, JN-RM-1022-20. https://doi.org/10.1523/jneurosci.1022-20.2020

Sharma, A. v., Nargang, F. E., & Dickson, C. T. (2012). Neurosilence: Profound Suppression of Neural Activity following Intracerebral Administration of the Protein Synthesis Inhibitor Anisomycin. *The Journal of Neuroscience*, *32*(7), 2377–2387. https://doi.org/10.1523/JNEUROSCI.3543-11.2012

Squire, L. R., & Barondes, S. H. (1973). Memory impairment during prolonged training in mice given inhibitors of cerebral protein synthesis. *Brain Research*, *56*(C), 215–225. https://doi.org/10.1016/0006-8993(73)90336-3

Squire, L. R., & Barondes, S. H. (1974). Anisomycin, like other inhibitors of cerebral protein synthesis, impairs 'long-term' memory of a discrimination task. *Brain Research*, *66*(2), 301–308. https://doi.org/10.1016/0006-8993(74)90148-6

Sweis, B. M., Mau, W., Rabinowitz, S., & Cai, D. J. (2021). Dynamic and heterogeneous neural ensembles contribute to a memory engram. *Current Opinion in Neurobiology*, *67*, 199–206. https://doi.org/10.1016/j.conb.2020.11.017

Vöröslakos, M., Petersen, P. C., Vöröslakos, B., & Buzsáki, G. (2021). Metal microdrive and head cap system for silicon probe recovery in freely moving rodent. *ELife*, *10*. https://doi.org/10.7554/eLife.65859

Wang, M. E., Wann, E. G., Yuan, R. K., Ramos Álvarez, M. M., Stead, S. M., & Muzzio, I. A. (2012). Long-term stabilization of place cell remapping produced by a fearful experience. *The Journal of Neuroscience*, *32*(45), 15802–15814. https://doi.org/10.1523/JNEUROSCI.0480-12.2012

Wood, E. R., Dudchenko, P. A., & Eichenbaum, H. B. (1999). The global record of memory in hippocampal neuronal activity. *Nature*, *397*(6720), 613–616. https://doi.org/10.1038/17605

Yger, P., Spampinato, G. L. B., Esposito, E., Lefebvre, B., Deny, S., Gardella, C., Stimberg, M., Jetter, F., Zeck, G., Picaud, S., Duebel, J., & Marre, O. (2018). A spike sorting toolbox for up to thousands of electrodes validated with ground truth recordings in vitro and in vivo. *eLife*, *7*, 1–23. https://doi.org/10.7554/eLife.34518

423

424 Methods:

425 **Animals**

426 Sixteen (n = 10 controls, 6 anisomycin) male C57/BL6 mice (Jackson Laboratories), age 16 to
427 22 weeks during behavioral and imaging experiments and weighing 25-32g were used in this
428 study. Three mice were excluded after performing this study: one mouse after histology
429 revealed the GRIN lens implant and viral expression to be medial to the intended imaging, while
430 the other two were excluded due to unstable/overexpression of GCaMP that produced aberrant
431 calcium activity which emerged toward the end of the experiment. After exclusion of these mice,
432 we retained 8 mice in the control (CTRL) group and 5 mice in the anisomycin group (ANI) group.
433 Additionally, behavioral video tracking files for one CTRL mouse were corrupted during
434 recording during all neutral field recordings from day 0 on: this mouse was excluded from all
435 analyses which required using behavior in the neutral arena (e.g., place field correlations and
436 any analyses where the CTRL group was split into Learners and Non-Learners). Mice were
437 socially housed in a vivarium on a 12 hour light-dark cycle with 1-3 other mice prior to surgery
438 and were housed singly thereafter. Mice were given free access to food and water throughout
439 the study. All procedures were performed in compliance with the guidelines of the Boston
440 University Animal Care and Use Committee.

441 One male Long Evans rat, 10 months old and weighing ~480g, was used for the
442 electrophysiological recording in this study. Rats were socially housed in a vivarium on an
443 adjusted 12 hour light-dark cycle (lights on at noon, off at midnight) with 1-3 other rats prior to
444 surgery and given free access to food and water throughout the study. All procedures were
445 performed in compliance with the guidelines of the University of Michigan Animal Care and Use
446 Committee.

447 **Viral Constructs**

448 For mice experiments we used an AAV9.*Syn*.GcaMP6f.WPRE.SV40 virus from the University of
449 Pennsylvania Vector Core/Addgene with an initial titer of ~$4x10^{12}$ GC/mL and diluted it into
450 sterilized potassium phosphate buffered saline (KPBS) to a final titer of ~$2\text{-}4x10^{12}$ GC/mL for
451 injection.

452 For rat experiments, we used an pGP.AAV9.*Syn*.GcaMP7f.WPRE.SV40 virus from the
453 University of Pennsylvania Vector Core/Addgene with an initial titer of $2.6x10^{13}$ GC/mL and
454 diluted it into sterilized phosphate buffered saline (PBS) to a final titer of $2.6x10^{12}$ GC/mL for
455 injection. Due to poor expression no imaging was performed.

456 **Stereotactic Surgery**

457 We performed two stereotactic surgeries and one base-plate implant on naïve mice, aged 3-8
458 months, according to previously published procedures (Kinsky et al., 2018; Resendez et al.,
459 2016). Both surgeries were performed under 1-2% isoflurane mixed with oxygen. Mice were
460 given 0.05mL/kg buprenorphine (Buprenex) for analgesia (subcutaneously, SC), 5.0mL/kg of
461 the anti-inflammatory drug Rimadyl (Pfizer, SC), and 400mL/kg of the antibiotic Cefazolin
462 (Pfizer, SC) immediately after induction. They were carefully monitored to ensure they never
463 dropped below 80% of their pre-operative weight during convalescence and received the same
464 dosage of Buprenex, Cefazolin, and Rimadyl twice daily for three days following surgery. In the

465 first surgery, a small craniotomy was performed at AP -2.0, ML +1.5 (right) and 250nL of
466 GcaMP6f virus (at the titer noted below) was injected 1.5mm below the brain surface at
467 40nL/min using a 1μL Hamilton syringe and infusion pump. The needle remained in place a
468 minimum of 10 minutes after the infusion finished at which point it was slowly removed, the
469 mouse's scalp was sutured, and the mouse was removed from anesthesia and allowed to
470 recover.

471 3-4 weeks after viral infusion, mice underwent second surgery to attach a gradient index (GRIN)
472 lens (GRINtech, 1mm x 4mm). After performing an ~2mm craniotomy around the implant area,
473 we carefully aspirated cortex using blunted 25ga and 27ga needles under constant irrigation
474 with cold, sterile saline until we visually identified the medial-lateral striations of the corpus
475 callosum. We carefully removed these striations using a blunted 31ga needle while leaving the
476 underlying anterior-posterior striations intact, after which we applied gelfoam for 5-10 minutes to
477 stop any bleeding. We then lowered the GRIN lens to 1.1mm below bregma. Note that this
478 entailed pushing down ~50-300μm to counteract brain swelling during surgery. We then applied
479 Kwik-Sil (World Precision Instruments) to provide a seal between skull and GRIN lens and then
480 cemented the GRIN lens in place with Metabond (Parkell), covered it in a layer of Kwik-Cast
481 (World Precision Instruments), and then removed the animal from anesthesia and allowed him
482 to recover after removing any sharp edges remaining from dried Metabond with a dental drill
483 and providing any necessary sutures.

484 Finally, after ~2-4 weeks we performed a procedure in which the mouse was put under
485 light anesthesia to attach a base plate for easy future attachment of a miniature epifluorescence
486 microscope (Ghosh et al., 2011, Inscopix, Inc.). Importantly, no tissue was cut during this
487 procedure. After induction, we attached the base plate to the camera via a set screw, set the
488 camera's focus level at ~1/3 from the bottom of its range, and carefully lowered the camera
489 objective and aligned it to the GRIN lens by eye, and visualized fluorescence via nVistaHD until
490 we observed clear vasculature and putative cell bodies expressing GcaMP6f (Resendez et al.,
491 2016). To counteract downward shrinking during curing, we then raised the camera up ~50μm
492 before applying Flow-It ALC Flowable Composite (Pentron) between the underside of the
493 baseplate and the cured Metabond on the mouse's skull. After light curing, we applied opaque
494 Metabond over the Flow-It ALC epoxy to the sides of the baseplate to provide additional
495 strength and to block ambient light infiltration. Mice were allowed to recover for several days
496 prior to habituation to camera attachment and performance of the behavioral task outlined
497 below. In the event that we did not observe clear vasculature and cell bodies when we first
498 visualized fluorescence we covered the GRIN lens with Kwik-Cast and removed the mouse from
499 anesthesia without attaching the baseplate. We then waited an additional week and repeated
500 the steps above.

501 For rats, we performed two surgeries in a similar manner as described above for mice.
502 However, rats were administered pre-operative and post-operative Meloxicam orally for
503 analgesia (in lieu of Buprenex) and triple-antibiotic was applied locally (in lieu of Cefazolin
504 injections) to the incision at the end of surgery. Meloxicam was additionally administered for two
505 days post-surgery during recovery, and animals were monitored daily for a minimum of seven
506 days during recovery. 0.4mL of a lidocaine/bupivacaine cocktail were given under the scalp to
507 provide local anesthesia at the incision site. In the first surgery, 1000nL of GcaMP7f virus was
508 infused in the prelimbic cortex at the center of a 1mm craniotomy (AP + 2.9, ML + 3.6, from
509 Bregma, DV -3.0 at an 18 degree angle from top of brain). Following infusion, ~1.5 mm of

510 overlying cortex was removed and a 23ga needle was lowered to ~500µm above the target site.
511 Then, a 0.6 x 7 mm GRIN lens was lowered to 3.0mm below the top of the brain, the area
512 between the skull and lens was sealed with Kwik-Sil, and the lens was affixed to the skull with
513 Vivid-Flow light-curable composite (Pearson Dental) and Metabond (Parkell). The lens was then
514 covered in Kwik-Sil for protection. During this surgery, ground and reference screws were also
515 placed over the cerebellum and a 3d printed crown base was attached to the rat's skull
516 (Vöröslakos et al., 2021) to which crown walls and top were connected and to further protect the
517 lens and future microdrive/probe implant. The rat was screened for fluorescence 8-12 weeks
518 later, but no cell dynamics were observed so no imaging equipment was implanted for this rat.

519 16 weeks later, the rat was again given pre-operative Meloxicam and anesthetized under
520 isoflurane. The crown walls were removed and a 1.0mm craniotomy was performed at AP-4.8,
521 ML+3.6 from bregma. After removing dura and stopping bleeding with cold, sterile saline, a
522 NeuroNexus A1x32-5mm-50-177 probe, attached to a metal microdrive, was implanted at 2.3
523 mm below the brain surface and the metal drive base was attached to the skull with Unifast light
524 cured dental epoxy (Henry-Schein). The craniotomy was sealed with Dow-Sil, the probe was
525 protected with dental wax, and the ground and reference wires were connected to the probe
526 electronic interface board (EIB). The crown walls were re-attached, the EIB was connected to
527 the crown walls, and the rat was removed from isoflurane and allowed to recovery. The rat was
528 monitored daily for 7 days prior to recording, during which the probe was lowered ~1mm until
529 sharp wave ripples and spiking activity were visualized indicating localization of the probe in the
530 CA1 cell layer.

531 **Histology procedures**

532 Hippocampal slices were prepared following extraction from mice in accordance with the
533 standard methods and guidelines of the Boston University Animal Care and Use Committee. In
534 brief, mice were euthanized with Euthasol (Virbac), transcardially perfused with
535 paraformaldehyde (PFA), and decapitated. Following extraction, brains were placed in PFA for
536 approximately 48 hours before undergoing sectioning. Brains that were sliced using a Cryostat
537 underwent an additional step of sucrose cryoprotection and subsequent freezing in -80C. Brains
538 were mounted to the slicing platform using Tissue Tek O. C. T. (Sakura) and kept at -30C
539 throughout sectioning. 50µm slices were collected across the entire aspiration site in the dorsal
540 hippocampus region. Brains that were sliced using a vibratome were stabilized using super glue
541 and submerged in 1% PBS. A Leica VT1000 S vibratome was equipped with a platinum coated
542 double edged blade (Electron Microscopy Sciences , Cat. #72003-01) and set to a maximal
543 speed of 0.9mm/s for collecting 50 µm slices. Slices prepared from both the cryostat and
544 microtome were directly mounted onto (type of slides go here) and cover-slipped using DAPI
545 following sectioning. No histology was performed in the rat study.

546 **Behavioral Paradigm**

547 Prior to surgery mice were handled to habituate them subsequent camera attachment. 3-7 days
548 following base plate attachment surgery we conditioned mice to the imaging procedures by
549 further handling them for 5-10 minutes for a minimum three days. During this handling a plastic
550 "dummy" microscope (Inscopix) of approximately the same size/weight as the imaging camera
551 was attached to each mouse's head and remained on his head for 1-2 hours in his home cage.
552 When it became easy to attach the scope to the mouse's head a real imaging miniscope was
553 attached to head and an optimal focus plane chosen. We then recorded three 5 minute imaging

554 videos at this focus and +/- ¼ turn (~25µm) in the mouse's home cage. These movies were
555 processed as described in the Image Acquisition and Processing section and an optimal zoom
556 was chosen based on whichever focus plane maximized cell yield and produced clear looking
557 cell bodies. Animals were then placed in a novel environment with a different size and shape
558 compared to the experimental environments for a 10 minute session to habituation them to the
559 general experimental outline and ensure that they explored novel arenas.

560 Following habituation to the imaging procedures mice performed a contextual fear
561 conditioning (CFC) task with simultaneous imaging of hippocampus neurons over the course of
562 10 days. Note that all recording sessions are referred to by their time relative to applying the
563 mild foot-shock and the arena in which the recording occurred: e.g., Shock Day -2 occurred in
564 the shock arena two days prior to foot-shock while Neutral 4 hours occurred four hours after
565 foot-shock in the neutral arena. A typical day (Days -2, -1, 1, 2, and 7) consisted of two separate
566 10 minute recording blocks/sessions: one in the Neural arena and one in the shock arena. Mice
567 first explored a square (neutral) arena, placed in the center of a well-lit room, for 10 minutes.
568 The neutral arena was a square constructed of 3/8" plywood (25cm x 25cm x 15 cm), which was
569 painted yellow with sealable paint. Additionally, one wall was painted with black horizontal
570 stripes for visual orientation purposes. The neutral arena was wiped down with 70% ethanol ~10
571 minutes prior to recording. After 10 minutes of exploration the experimenter took the mouse out
572 of the arena, leaving the miniscope camera on their head and placed the mouse in its home
573 cage on a moveable cart upon which it was immediately transported down a short hallway to
574 second room.

575 The second room was dimly lit and contained the fear conditioning (shock) arena. The
576 shock arena (Coulbourn Instruments, Whitehall, PA, USA) consisted of metal-panel side walls,
577 Plexiglas front and rear walls, and a stainless-steel grid floor composed of 16 grid bars (22cm x
578 22cm). Following 10 minutes of exploration of the shock arena, mice were removed from the
579 arena, the camera was removed, and mice were returned to their home cage. Both arenas were
580 wiped down with 70% ethanol ~10min prior to recording to eliminate any odor cues. Note that
581 mice always explored the neutral arena first and the shock arena second. For the Day 0
582 sessions, mice first explored the neutral arena for 10 minutes and were transported to the shock
583 arena as usual. However, during this session (Shock Day 0) the mouse was immediately given
584 a single 0.25mA shock and allowed to explore the arena for an additional 60 seconds only
585 before being removed and returned to his cage. Efficacy of shock was confirmed post-hoc by
586 eye by the presence of jumping/darting behavior immediately post-shock. The 4 hour session
587 was identical to the Day -2, 1, 1, 2, and 7 sessions. With the exception of the 4 hour session, all
588 recording sessions were performed in the first half of the mouse's life cycle while the 4 hour
589 session occurred in the second half of the light cycle.

590 On day zero, after the camera was removed and prior to returning to their home cage, mice
591 received an intraperitoneal injection of either anisomycin (150 mg/kg, Sigma-Aldrich A9789) or
592 the equivalent amount of vehicle. After injection, they were returned to their cage for 4 hours
593 until the next recording session began.

594 Following extensive habituation to a rest box during the seven day recovery period, rat neural
595 activity and behavior was recorded across ~ 5 hours. Following a 15 minute baseline recording
596 (PRE) in the rest box, the animal was given an I.P. injection of anisomycin and then immediately
597 placed on a novel linear track which he explored for 45 minutes (TRACK). The rat was then
598 placed back into the rest box for 3.5 hours (POST). Following that, the animal was placed on a

599 second novel track for 45 minutes (TRACK) followed by a brief recording in the rest box
600 (POST2). Data was acquired continuously throughout with the exceptions of periodic cable
601 disconnections to perform the I.P. injection, start a new recording epoch, and
602 disconnect/reconnect cables that became twisted.

603 **Anisomycin**

604 For mice recordings, 25 mg of anisomycin was dissolved into 50 µL of 6N HCl and 500 µL of
605 1.8%NaCl. ~125 µL of 1N NaOH was then added to the solution followed by 0.1-0.5 µL of 1N
606 NaOH, testing pH after each addition until a final pH of 7.0 to 7.5 was reached, with a final
607 concentration of 24-27 mg/mL. In the case that pH rose above 7.5 during titration and and/or the
608 anisomycin went back into precipitate, small amounts (10-20 µL) of 6N HCl were added until
609 particles were no longer visible and the titration with 1N NaOH was restarted. Mice were
610 administered 150mg/kg of anisomycin solution via intraperitoneal injection, or ~0.15-0.18mL for
611 a typical 30g mouse.

612 For rat recordings, 100mg of anisomycin was dissolved into 1.6mL of 0.1N HCl (in 0.9% saline).
613 ~240 µL of 1N HCl was added, then 10-12 µL of NaOH was added in 1-2 µL amounts, testing
614 pH between each step until a pH of 7-7.5 was reached. 0.9% Saline was then added until a final
615 concentration of 33 mg/mL was reached. Due to a small amount of waste, the final amount
616 injected was 50mg (1.5 mL) which corresponds to 100 mg/kg for the rat.

617 **Behavioral Tracking and Fear Metrics**

618 We utilized two different camera/software configurations for tracking animal behavior. Both
619 configurations generated a TTL pulse at the beginning of behavioral tracking to synchronize with
620 image acquisition. We utilized Cineplex software (v2, Plexon) to track animal location at 30Hz in
621 the neutral arena. We used FreezeFrame (Actimetrics) to track animal location in the shock
622 arena at 3.75Hz. Animal location was obtained post-hoc via custom-written, freely available
623 Python software (www.github.com/wmau/FearReinstatement). We observed inconsistent frame
624 rates and inaccurate acquisition of behavioral video frames for one mouse in the neutral arena
625 during the day 0, 4 hour, and day 1-2 sessions. These sessions were excluded from analysis.

626 Freezing was calculated by first dowsampling neutral position data to 3.75 Hz to match the
627 sample rate used in the shock arena. We then identified freezing epochs as any periods of 10
628 consecutive frames (2.67 seconds) or more where the mouse's velocity was less than
629 1.5cm/second.

630 **Neural Discrimination**

631 We evaluated the extent to which each animal's behavior reflected the expression of a context-
632 specific fear memory through a behavioral discrimination index (DI_{beh}), calculated as follows:

633 $$DI_{beh} = \frac{Frz_{Neutral} - Frz_{Shock}}{Frz_{Neutral} + Frz_{Shock}}$$

634 Where $Frz_{Neutral}$ and Frz_{Shock} are the percentages of time spent freezing in the neutral and shock
635 arenas, respectively. Thus, a negative DI_{beh} value indicated more freezing behavior in the shock
636 arena (indicating successful encoding of a context-specific fear memory), a positive DI_{beh} value
637 indicated more freezing behavior in the neutral arena, and a DI_{beh} value around zero indicated

equal/low freezing behavior in each arena (indicating the formation of a non-specific or weak fear memory).

Imaging Acquisition and Processing

Brain imaging data was obtained using nVista HD (Inscopix) at 720 x 540 pixels and a 20 Hz sample rate. Note that imaging data for one mouse was obtained at 10 Hz. Prior to neuron/calcium event identification we first pre-processed each movie using Inscopix Imaging Suite (Inscopix) software. Preprocessing entailed three steps a) motion corrections, and b) cropping the motion-corrected movie to eliminate any dead pixels or areas with no calcium activity, and c) extracting a minimum projection of the pre-processed movie for later neuron registration. We did not analyze one imaging session in which we had to reconnect the camera cable mid-session and could not synchronize the imaging data with behavioral data. Maximum projections of imaging movies were made using the Inscopix Imaging Suite or custom-written functions based off of an open-source MATLAB library (Muir & Kampa, 2015).

Electrophysiological Recordings

Data was acquired using an Intan 1028 channel recording system through OpenEphys software into binary format and behavior was tracked via Omnitrack high resolution cameras.

Data Analysis

Data analysis was performed in both Python and MATLAB software. Python analysis code is available at https://github.com/nkinsky/Eraser.

Spike sorting and analysis

Electrophysiological recordings were automatically clustered using SpyKING CIRCUS software (Yger et al., 2018) and units were manually curated in phy. Units were grouped into single units if they exhibited a clear refractory period and were well-isolated from other putative spikes. Other units which exhibited a clear waveform but were either poorly isolated or exhibited refractory period violations were classified as multi-unit activity (MUA). All single units and MUA were combined and cross-correlograms for the combined activity were created for each epoch of the recording separately.

Tenaspis

Neuron regions-of-interest (ROIs) and calcium events were identified using a custom written, open source algorithm employed in MATLAB 2016b called A Technique for Extracting Neuronal Activity from Single Photon Neuronal Image Sequences (Tenaspis) (Mau et al., 2018). This procedure was comprehensively documented in Kinsky et al., 2018:

"Tenaspis is open-source and available at: https://github.com/SharpWave/TENASPIS. First, Tenaspis filters each calcium imaging movie with a band-pass filter per (Kitamura et al., 2015) to accentuate the separation between overlapping calcium events. Specifically, Tenaspis smooths the movie with a 4.5 μm disk filter and divides it by another movie smoothed with a 23.6 μm disk filter. Second, it adaptively thresholds each imaging frame to identify separable pockets of calcium activity, designated as blobs, on each frame. Blobs of activity are accepted at this stage of processing only if they approximate the size and shape of a mouse hippocampal neuron, as measured by their radius (min = ~6μm, max = ~11μm), the ratio of long to short axes (max = 2), and solidity (min = 0.95), a metric used by the *regionprops* function of MATLAB we

679 employ to exclude jagged/strange shaped blobs. Third, Tenaspis strings together blobs on
680 successive frames to identify potential calcium transients and their spatial activity patterns.
681 Fourth, Tenaspis searches for any transients that could results from staggered activity of two
682 neighboring neurons. It rejects any transients whose centroid travels more than 2.5μm between
683 frames and whose duration is less than 0.20 seconds. Fifth, Tenaspis identifies the probable
684 spatial origin of each transient by constructing putative regions-of-interest (ROIs), defined as all
685 connected pixels that are active on at least 50% of the frames in the transient. Sixth, Tenaspis
686 creates initial neuron ROIs by merging putative transient ROIs that are discontinuous in time but
687 occur in the same location. Specifically, it first attempts to merge all ROIs whose centroids are
688 less than a distance threshold of ~0.6μm from each other. In order to merge two transient ROIs,
689 the two-dimensional Spearman correlation between the ROIs must yield $r^2 > 0.2$ and $p < 0.01$.
690 Tenaspis then successively increases the distance threshold and again attempts to merge ROIs
691 until no more valid merges occur (at a distance threshold of ~3μm, typically). Seventh, Tenaspis
692 integrates the fluorescence value of each neuron ROI identified in the previous step across all
693 frames to get that neuron's calcium trace, and then identifies putative spiking epochs for each
694 neuron. Specifically, it first identifies the rising epochs of any transients identified in earlier
695 steps. Then, it attempts to identify any missed transients as regions of the calcium trace that
696 have a) a minimum peak amplitude > 1/3 of the transients identified in step 3, b) a high
697 correlation ($p < 0.00001$) between active pixels and the pixels of the average neuron ROI
698 identified in step 6, and b) a positive slope lasting at least 0.2 seconds. Last, Tenaspis searches
699 for any neuron ROIs that overlap more than 50% and whose calcium traces are similar and
700 merges their traces and ROIs."

701 **Between Session Neuron Registration**

702 We utilized custom-written, freely available MATLAB code (available at
703 https://github.com/nkinsky/ImageCamp) to perform neuron registration across sessions in
704 accordance with previous results (Kinsky et al., 2018). The details of this procedure described in
705 Kinsky et al. (2018) are reproduced here:

706 "Neuron registration occurred in two steps: session registration and neuron registration.

707 *Session registration* – Prior to mapping neurons between sessions, we determined how
708 much the imaging window shifted between sessions. In order to isolate consistent features of
709 the imaging plane for each mouse (such as vasculature or coagulated blood), we created a
710 minimum projection of all of the frames of the motion-corrected and cropped brain imaging
711 movie for each recording session. One session ("registered session") was then registered to a
712 base session using the "imregtform" function from the MATLAB Image Processing Toolbox,
713 assuming a rigid geometric transform (rotation and translation only) between images, and the
714 calculated transformation object was saved for future use.

715 *Neuron Registration* – Next, each ROI in the registered session was transformed to its
716 corresponding location in the base session. Each neuron in the base session was then mapped
717 to the neuron with the closest center-of-mass in the registered session, unless the closest
718 neuron exceeded our maximum distance threshold of 3 pixels (3.3 μm). In this case the base
719 session neuron was designated to map to no other neurons in the registered session. If, due to
720 high density of neurons in a given area, we found that multiple neurons from the base session
721 mapped to the same neuron in the registered session, we then calculated the spatial correlation

(Spearman) between each pair of ROIs and designated the base session ROI with the highest correlation as mapping to the registered session ROI.

For multiple session registrations, the same procedure as above was performed for each session in two different ways. First, we registered each session directly to the first session in the experiment and updated ROI locations/added new ROIs to set of existing ROIs with each registration. This helped account for slight day-to-day drift in neurons ROIs due to shifts in vasculature, build-up of fluid underneath the viewing window, creep/shrinkage of dental cement, etc. Second, to ensure that neuron ROIs did not drift excessively across sessions we also performed all the above steps but did NOT update ROI locations allowing us to register each set of ROIs to those furthest away chronologically. The resulting mappings were then compared across all sessions, and any neuron mappings that differed between the two methods (e.g., ROIs that moved excessively across the duration of the experiment) were excluded from analysis. Those that remained in the same location were included."

The procedure to assess the quality of across session registration was described in Kinsky et al. (2018) and is reproduced here: "We checked the quality of neuron registration between each session-pair in two ways: 1) by plotting the distribution of changes in ROI orientations between session and comparing it to chance, calculated by shuffling neuron identity between session 1000 times, and 2) plotting ROIs of all neurons between two sessions and looking for systematic shifts in neuron ROIs that could lead to false negatives/positives in the registration." All session-pairs (except those few in which we could not synchronized imaging and behavioral data as noted above) met the above two criteria and were thus included in our analysis.

Cells that had calcium activity in the first session (neutral arena) for which we did not identify a matching neuron in the second session (shock arena) were classified as OFF cells. Likewise, neurons active in the shock arena with no matching partner in the neutral arena were classified as ON cells.

All neuron registrations were cross validated by overlaying ROIs from each session and evaluating their match by eye. In a few cases, we noticed erroneous registrations and adjusted our between-session neuron alignment by calculating the rigid geometric transformation using 4-5 cell ROIs active in both sessions.

Neural Discrimination Metrics

The extent to which gross hippocampal ensemble activity differed between arenas was calculated in two ways. First, we calculated the proportion of cells that turned ON and OFF between arenas divided by the total number of cells active in either arena.

Next, we calculated the extent to which each neuron active in both arenas distinguished between arenas by changing its event rate in a manner analogous to $DI_{Fr.}$ However, we took the absolute value to account for the fact that both positive and negative event rate changes could reflect neural differentiation between arenas. Then, we took the mean across all neurons to obtain a neural discrimination index (DI_{Neuron}):

$$DI_{Neuron} = \left| \frac{ER_{Neutral} - ER_{Shock}}{ERz_{Neutral} + ER_{Shock}} \right|$$

Placefield Analysis

Calcium transients occurring when the mouse was running greater than or equal to 1.5cm/second were spatially binned (1cm by 1cm) and occupancy normalized following which place fields were identified and quantified in a manner similar to Kinsky et al. (2018), reproduced here:

"Spatial mutual information (SI) was computed from the following equations, adapted from (Olypher et al., 2003)

$$I_{pos}(x_i) = \sum_{k=0}^{1} P_{k|x_i} \, log \left(\frac{P_{k|x_i}}{P_k}\right)$$

$$SI = \sum_{i=1} P_{x_i} \, I_{pos}(x_i)$$

where:

- P_{xi} is the probability the mouse is in pixel x_i
- P_k is the probability of observing *k* calcium events (0 or 1)
- $P_{k|xi}$ is the conditional probability of observing *k* calcium events in pixel x_i.

The SI was then calculated 1000 times using shuffled calcium event timestamps, and a neuron was classified as a place cell if it 1) had at least 5 calcium transients during the session, and 2) the neuron's SI exceeded 95% of the shuffled Sis…We defined the extent of a place field as all connected occupancy bins whose smoothed event rate exceeded 50% of the peak event rate occupancy bin."

Since spatial mutual information is biased by the number of samples (Olypher et al., 2003), we re-sampled the behavioral tracking data to match that of the imaging data (20Hz). This required up-sampling the shock arena data (3.75Hz->20Hz) and down sampling the neutral arena data (30Hz->20Hz).

Placefield similarity between sessions was assessed by first smoothing the 2-d occupancy normalized event rate maps with a gaussian kernel (2.5cm std), flattening the smoothed maps into a vector, and then performing a Spearman correlation between all neurons active in both sessions. To quantify chance-level place field similarity we randomly shuffled the mapping between neurons from the first to the second session before performing the Spearman correlation. We then repeated this procedure 100 times.

To assess the possibility that the configuration of place fields rotated together coherently between sessions (Kinsky et al., 2018), we again performed a Spearman correlation but after rotating the 2-d occupancy map in the second session 90 degrees. Since, due to small camera distortions, some 2-d occupancy maps were not square, one some occasions we resized (minimally) the second map to match the size/shape of the first map using the reshape function in Python's numpy package prior to correlate the two maps. We repeated this in successive 90 degree increments and then took the mean correlation of all neurons that were active in both

sessions to determine the optimal/“best” rotation of the place field map as that which maximized the correlation between sessions.

We also performed a “center-out” rotation analysis to assess coherent place field rotations between sessions. First, the angle to the pixel with the maximum occupancy normalized event rate was identified for each cell. Second, this angle was recalculated for the same cell in a different session in the same box. These two angles were subtracted to get the “center-out” rotation between sessions. Sessions which exhibited a coherent rotation displayed a peak in a histogram of center-out angles at 0, 90, 180, or 270 degrees, while sessions which exhibited global remapping exhibited a uniform distribution of rotation angles.

Freeze-tuned Cell Analysis

Freeze onset and offset times were first identified for each mouse/session as noted in the *Behavioral Tracking and Fear Metrics* section above. We then formed calcium event rasters using the neural activity for each cell +/- 2 seconds from freeze onset, organizing the data into a *nfreeze_onsets x ntime_bins* array. We then summed this raster along the 0th dimension to get a freeze tuning curve. To calculated significance, we randomly, circularly shifted the putative spiking activity for a cell and calculated a shuffled tuning curve in a similar manner to the actual data. We repeated this procedure 1000 times, and calculated significance for each time bin as the number of shuffles where the shuffled tuning exceeded the actual tuning curve divided by 1000. Last, we designated cells as significantly freeze-tuned if they had 3 or more bins with $p < 0.01$ and were active on at least 25% of freezing events.

Covariance Analysis

Putative spiking activity for each cell was first binned into 0.5 second windows and z-scored after binning, forming a *ncells x nbins* array. The covariance of this array was then calculated using the *cov* function in numpy. For between-session comparisons, cells active in both sessions were matched up and a new array was formed with the base (1st) session covariance in the lower diagonal and the registered (2nd) session in the upper diagonal. All entries along the main diagonal were ignored.

<u>Author Contributions</u>

Conceptualization: N.R.K with the help of Howard Eichenbaum; Methodolgy: N.R.K; Software: N.R.K., E.A.R; Validation: N.R.K; Formal Analysis: N.R.K, D.O.O., E.A.R; Investigation: N.R.K., D.O.O., E.A.R.; Data Curation: N.R.K., D.O.O., E.A.R.; Writing – original draft preparation: N.R.K.; Writing – review and editing; N.R.K, D.O.O, E.A.R., K.D., S.R.; Visualization: N.R.K.; Project Administration; N.R.K, S.R.; Funding Acquisition: N.R.K., K.D., S.R.

<u>Competing Interests</u>

The authors declare no competing interests.

835 FIGURE LEGENDS

836 **Figure 1: Neural discrimination between arenas predicts specificity of fear learning. A)** Schematic
837 of the behavioral paradigm. Mice freely explored two distinct arenas (neutral and shock) for 10 minutes
838 each day. Mice underwent mild contextual fear conditioning on day 0 in the shock arena followed by
839 immediate I.P. administration of anisomycin or vehicle in their home cage. Memory recall tests were
840 conducted 4 hours and 1, 2, and 7 days post-shock. The time of each session is referenced to the shock
841 session. **B)** (left) Learner (CTRL) mice freezing on all days. Red = shock arena, blue = neutral arena.
842 *p=1.3e-0.5 shock – neutral freezing from days -2/-1 to days ½ one-sided t-test (n=4 mice). (right) Same
843 but for Non-Learner (CTRL) mice (n=3 mice). **C)** (left) Neural overlap plots between neutral and shock
844 arenas for an example Learner mouse on day -1, before shock. Green = cells active in the shock arena
845 only, yellow = cells active in the neutral arena only, orange = cells active in both arenas. (right) Same for
846 example Non-Learner on day -2 showing higher overlap of active cells between arenas. **D)** Same as B
847 but for ANI group **E)** Mean neural discrimination between arenas (same day, days -2 to -1 and 1 to 2) vs.
848 within arenas (same arena, days -2 and -1, days 1 and 2). *p=2.35e-8 (ρ=-0.56) Spearman correlation**. F)**
849 Example calcium activity from the Learner mouse shown in C (left) for cells active in both arenas. Black =
850 calcium trace, red = putative spiking activity during transient rises. Top row shows shock arena preferring
851 cells, bottom row shows neutral arena preferring cells. **G)** Behavioral discrimination between arenas after
852 shock (Days 1-2) shows formation of a specific fear memory for Learners only, by definition (positive =
853 more freezing in neutral arena, negative = more freezing in shock arena, 0 = equal freezing in both
854 arenas). *p=0.022, **p=0.00038 1-sided t-test **H)** Neural discrimination between arenas BEFORE shock
855 indicates Learners formed more distinct representations of each arena prior to learning. Same
856 conventions as F. *p=0.030, +p=0.059 two-sided t-test. **I)** Neural overlap between arenas correlates with
857 specificity of fear memory on days 1-2 for Learners but not Non-Learners. *p=0.033 (ρ=0.61). **J)** Same as
858 I) but plotting neural overlap vs. behavioral discrimination between arenas. +p=0.059 (ρ=-0.56) for
859 Learners.

860 **Figure 2: Anisomycin accelerates cell turnover and stifles learning-related place field remapping**
861 **A)** Cell overlap ratio with Day -2 session, CTRL group. Blue = within shock arena, red = shock v. neutral
862 arena. **B)** Same as A) but for ANI group. **C)** Change in overlap ratios from a and b. *p=0.028,
863 **p=0.00024 two-sided t-test. **D)** Number of active neurons observed each day, normalized to day -1.
864 *p=0.039 two-sided t-test. **E)** Stable place field. (*top)* Example mouse trajectory (black) with calcium
865 activity (red) overlaid for the same cell from day -2 to -1 in shock arena, *(bottom)* occupancy normalized
866 rate maps for the same cells. **F)** Remapping place field. Same as E) but for a different cell that remaps
867 from day -2 to day 1 in the shock arena. **G)** Place field correlations for all mice before shock (Days -2 and
868 -1). *p<0.0032 Learners vs ANI and Non-Learners vs ANI, **p=1.9e-6 Non-Learners vs ANI, k-s test after
869 Bonferroni correction. **H)** Same as G) but for days after shock. *p=0.045 Learners vs Non-Learners and
870 p=0.0059 Non-Learners vs ANI, +p=0.1 Learners vs ANI. **I)** Same as G) but to assess learning-related
871 remapping from before to after shock. *p=0.00021 Learners vs Non-Learners and p=3.4e-11 Non-
872 Learners vs ANI, +p=0.12 Learners vs ANI. **J)** Place field correlations before shock broken down by
873 mouse. **K)** Same as J) but for sessions after shock. **L)** Same as J) but from before to after shock. p=0.002
874 mixed ANOVA, group x arena interaction. *p=0.025 Non-Learners vs ANI, **p=0.013 Learners vs Non-
875 Learners, ***p=0.034 Learners vs ANI, post-hoc pairwise t-test after Bonferroni correction.

876 **Figure 3: ANI administration suppresses the development of coordinated freeze-related neural**
877 **activity**. **A) and B)** Example traces from two freeze-cells which exhibit coordinated activity prior to
878 freezing event during the day 1 memory recall session in the shock arena. Red = putative spiking activity,
879 pink = cell shown in C, blue = cell shown in E. **C)** Proportion of freeze-tuned cells detected each day
880 across all groups. Green = freezing epochs. **D) and E)** Example Learner freeze-tuned cells identified
881 during the 4 hour (D) or day 1 (E) memory test tracked across sessions. Peri-event calcium activity
882 rasters are centered on freeze onset time (solid green). Dashed green = baseline calcium event
883 probability, red solid = peri-freeze calcium event probability, bins with p<0.01 (circular permutation test)
884 noted with red bars at top. D/E corresponds to pink/blue cells shown in A-B. Bold = session with
885 significant freeze-tuning. **F)** Same as D and E but for ANI mouse shock cell identified during the 4 hour
886 session. **G)** Change in peak peri-freeze calcium event probability for all freeze-tuned cells detected during

887 the 4 hour session. **H)** Same as G but for freeze-tuned cells detected during Day 1 recall session. p <
888 0.02 1-way ANOVA each day separately, *p=0.02, **p=0.001, ***p=0.0006 post-hoc Tukey test. **I)** Freeze-
889 tuned cells exhibit increased covariance in the CTRL compared to the ANI group. Mean covariance of
890 freeze-tuned cells from each session shown. p=0.016 two-way ANOVA (Time). *p=0.018 post-hoc
891 pairwise t-test (two-sided) after Bonferroni correction. **J)** Small but significant increase in covariance of all
892 cells for CTRL mice during the 1 day recall session. p=0.0015 (Time), 0.005 (Group), 0.036 (Group x
893 Time) two-way ANOVA. *p=0.014, **p=0.008, ***p=0.004 post-hoc pairwise t-test (two-sided) after
894 Bonferroni correction. **K)** Mean covariance of freeze-tuned cells detected during the 4 hour session
895 tracked across sessions. P=0.005 (Group), 0.04 (Group x Time) two-way ANOVA. *p=0.014 post-hoc
896 pairwise t-test (two-sided) after Bonferroni correction. **L)** Same as K but for freeze-tuned cells detected
897 during the day 1 recall session. p=0.0003 (Group) two-way ANOVA. *p=0.016 post-hoc pairwise t-test
898 (two-sided) after Bonferroni correction.

899

900 **Figure S1**: **CTRL animals exhibit behavioral variability following learning and similar rates of cell**
901 **turnover between arenas vs. across days.**

902 **A)** CTRL mice freezing on all days. Red = shock arena, blue = neutral arena *p=0.025 shock - neutral
903 freezing from days -2/-1 to days 1/2, one-sided t-test (n=7 mice). **B)** Distribution of DI_{beh} scores for all
904 mice in CTRL group on days 1 and 2. Dashed line indicates cutoff between Learners and Non-Learners.
905 **C)** Cell overlap 1 day apart in the same arena (days -2 to -1 and 1 to 2) vs. cell overlap between arenas
906 on the same day (days -2, -1, 1, 2) for all mice in CTRL group. *p=1.7e-5, r=0.74 Spearman correlation.

907

908 **Figure S2: Non-specific effects of Anisomycin include a reduction in locomotion**

909 **A)** 4 mice were given I.P injections of anisomycin only (no shock) and their locomotion was tracked over
910 24 hours. Normal activity did not return to baseline until between 6 and 24 hours later.

911

912 **Figure S3**: **Coherent Place Field Rotations Observed Between Sessions**

913 **A)** Example animal trajectories from neutral arena day -2 (top row) and day -1 (middle row) with calcium
914 activity overlaid (red). Each column corresponds to one cell. Bottom row shows data rotated 90 degrees,
915 demonstrating a coherent rotation of spatial activity for all neurons. **B)** Smoothed, occupancy normalized
916 calcium event maps corresponding to data shown in A). **C)** The angle from the center of the arena to
917 each cell's maximum intensity place field center was calculated for each session (center-out angle).
918 The distribution of center-out angles plotted, demonstrating a coherent rotation of place fields from Day -2
919 to Day -1 by 90 degrees. **D)** Place field correlations (smoothed event maps) between sessions indicate
920 apparently low stability across days without considering rotations, giving the false impression that the
921 place field map randomly reorganizes between sessions. **E)** High correlations were observed after
922 considering a coherent 90 degree rotation between sessions, indicating that place fields retain the same
923 relative structure but rotate together as a whole. **F)** Mean correlations for each mouse and **G)** combined
924 correlations for all neurons calculated without considering rotations gives the impression of instability
925 before/after shock and heightened remapping for all groups from before to after learning.

926

927 **Figure S4: Place field correlations with STM (4 hour) session**

928 **A)** Distribution of place field correlations for all mice combined for sessions before (Day -2 and Day -1) vs
929 4 hour session. **B)** Same as A) but for 4 hour vs days 1-2 sessions. *p=0.0217 Non-Learners v ANI in
930 shock arena, **p=0.00014 Non-Learners v ANI neutral arena, ***p=3.6e-8 Learners v Non-Learners
931 neutral Arena. All p-values after Bonferroni correction for 3 comparisons. **C)** Before v STM mean place
932 field correlations for each mouse/session-pair. **D)** Same as C but for STM v After.

933

934 **Figure S5: Population Vector (PV) correlations indicate that anisomycin disrupts cell turnover**

935 **A)-E)** 1D PV correlations between sessions including only cells active in BOTH sessions. **A)** Before (Days
936 -2 and -1), *p=0.006 shock v neutral arena, mixed ANOVA. **B)** After (Days 1 and 2) *p=0.024 shock v
937 neutral arena, mixed ANOVA. **C)** Before v After, p < 0.003 neutral v shock arena and Group x Arena
938 interaction, mixed ANOVA. *p<0.001, +p=0.056 t-test (two-sided) after Bonferroni correction. **D)** Before v
939 STM (4 hour), p=0.052 Group x Arena interaction, mixed ANOVA. **E)** STM v After *p=0.004 Neutral v
940 Shock arena, mixed ANOVA. **F)-J)** 1D PV correlations including cells active in EITHER session (includes
941 new and silent cells). **F)** Before *p<0.001 shock v neutral arena, mixed ANOVA. **G)** After, p > 0.12 all
942 comparisons mixed ANOVA. **H)** Before v After, p<0.003 all comparisons mixed ANOVA *p=0.023
943 Learners v ANI, **p=0.007 Non-Learners v ANI, +p=0.083 Non-Learners v ANI t-test (two-sided) after
944 Bonferroni correction. **I)** Before v STM p<0.005 Arena and Group comparisons, p=0.059 Arena x Group
945 interaction, *p=0.004 Learners v ANI, **p=0.033 Learners v ANI t-test (two-sided) after Bonferroni
946 correction. **J)** STM v After p<0.022 Arena and Group comparisons, p=0.103 Arena x Group interaction,
947 *p=0.041 Learners v ANI, **p=0.003 Non-Learners v ANI, ***p=0.003 Non-Learners v ANI t-test (two-
948 sided) after Bonferroni correction**.** Green = Learners, Orange = Non-Learners, Blue = ANI.

949

950 **Figure S6: Freeze-cell covariance increases are driven by Learners and not purely a result of less**
951 **freezing in Non-Learners and the ANI group.**

952 **A)-C)** Example freeze-tuned cells tracked across sessions forward and backward in time from the day
953 indicated in bold. Peri-event calcium activity rasters are centered on freeze onset time (solid green).
954 Dashed green = baseline calcium event probability, red solid = peri-freeze calcium event probability, bins
955 with p<0.01 (circular permutation test) noted with red bars at top. D/E corresponds to pink/blue cells
956 shown in A-B. **A)** Example cell from Non-Learner **B)-C)** Example cells from two different Learners. **D)**
957 Proportion freeze-tuned cells detected in neutral arena across days. **E)** Mean covariance of all cells in
958 neutral arena prior to learning exhibit small changes, compare y-axis to Figure 3J. p=0.012 two -way
959 ANOVA, *p=0.04 post-hoc pairwise two-sided t-test after Bonferroni correction. **F)** Mean covariance
960 freeze-tuned cells after randomly downsampling the number of freeze events to match the average
961 number observed during days -2 and -1. p=0.02 two-way ANOVA, +p= 0.055 post-hoc pairwise two-sided
962 t-test after Bonferroni correction, mean of 100 downsampling iterations. **G)** Same as F) but for all cells
963 p0.0015 two-way ANOVA, *p=0.02, **p=0.008, ***p=0.004 post-hoc pairwise two-sided t-test after
964 Bonferroni correction. **H)** Mean covariance of freeze cells excluding peri-freeze times (freeze start +/- 2
965 sec) from neural activity. P=0.012 (Time) two-way ANOVA. **I)** Same as H) but for all cells. p=0.001 (Time)
966 two-way ANOVA *p=0.045, **p=0.006, ***p=0.004 post-hoc pairwise t-test (two-sided). **J)** Mean
967 covariance of freeze cells before, 4 hours after, and 1-2 days after learning/ANI injection broken down by
968 learning group. p=0.014 (Time) two-way ANOVA. *p=0.04 post-hoc pairwise t-test (two-sided). **K)** Same
969 as J) but for all cells. p=0.0008 (Time) two-way ANOVA. *p=0.012, **p=0.0028 post-hoc pairwise t-test
970 (two-sided). **L)** Same as J) but tracking freeze-tuned cells from the 4 hour session forward/backward in
971 time. p=0.006 (Time) two-way ANOVA. +p=0.13 post-hoc pairwise t-test. **M)** Same as L) but for 1 day
972 freeze cells tracked forward/backward in time.

973

974 **Figure S7: Reduced activity following anisomycin administration is not an imaging artifact and**
975 **does not result from global disruption of electrical neural activity in hippocampal neurons.**

976 **A-C)** Neural activity was tracked across ~5 hours before and after systemic administration of anisomycin.
977 **A)** Cross correlograms for all single and multi-unit activity combined are shown from the pre epoch in a
978 rest box (15 minutes), running on a novel track immediately following anisomycin injection (45 minutes),
979 post epoch in the rest box (3.5 hours), running on a second novel track (45 minutes), and a second post
980 epoch in the rest box (15 minutes). Clear modulation of firing at the theta timescale is observed. **B)**

Example trace from electrode in pyramidal cell layer of CA1 showing theta activity 10 minutes and 4 hours 15 minutes post injection anisomycin injection. **C)** Example sharp wave ripple events occurring from 25 minutes to 4 hours 15 minutes post anisomycin injection.

D-E) The signal-to-noise ratio of all neurons captured using calcium imaging and active between sessions was tracked between sessions. **D)** Mean height of calcium transient peaks for all cells matched from day -1 to 4 hour session. $p>0.63$ both groups, two-sided t-test. **E)** Same as D) but tracking cells from day -1 to day 1, $p>0.68$ both groups.